

Getting the Most Neutrinos out of IsoDAR

Emilio Ciuffoli^{*}, Jarah Evslin[†], Hosam Mohammed[‡], Fengyi Zhao[§] and
Maksym Deliyergiyev[¶]

Institute of Modern Physics, CAS, NanChangLu 509, Lanzhou 730000, China

Abstract

Several experimental collaborations worldwide intend to test sterile neutrino models by measuring the disappearance of antineutrinos produced via isotope decay at rest (IsoDAR). The most advanced of these proposals have very similar setups, in which a proton beam strikes a target yielding neutrons which are absorbed by a high isotopic purity ${}^7\text{Li}$ converter, yielding ${}^8\text{Li}$ whose resulting decay yields the antineutrinos. In this note, we use FLUKA and GEANT4 simulations to investigate three proposed modifications of this standard proposal. In the first, the ${}^7\text{Li}$ is replaced with ${}^7\text{Li}$ compounds including a deuterium moderator. In the second, a gap is placed between the target and the converter to reduce the neutron bounce-back. Finally, we consider cooling the converter with liquid nitrogen. We find that these modifications can increase the antineutrino yield by as much as 50 percent. The first also substantially reduces the quantity of high purity ${}^7\text{Li}$ which is needed.

^{*}ciuffoli@impcas.ac.cn

[†]jarah@impcas.ac.cn

[‡]hosam@impcas.ac.cn

[§]fengchu@impcas.ac.cn

[¶]deliyergiyev@impcas.ac.cn

1 Introduction

1.1 Motivation

Various anomalies can be explained if one invokes sterile neutrinos. The most convincing of these is the LSND anomaly [1, 2], in which $\bar{\nu}_e$ appeared in a detector located 30 meters away from a μ^+ decay at rest $\bar{\nu}_\mu$ source. While the appearance signal is in nearly 4σ of tension with a three flavor mixing model, it is easily explained in the presence of a single flavor of sterile neutrino. However other appearance experiments in the same channel have produced negative [3, 4] or inconclusive [5] results. Anomalous disappearance of $\bar{\nu}_e$ produced by a radioactive source in a detector [6, 7], called the Gallium anomaly, can also be explained with a single flavor of sterile neutrino with a mass of at least 1 eV.

The anomalous disappearance of reactor neutrinos, called the reactor anomaly [8], can also be explained with a single sterile neutrino with a mass which may be as small as 0.1 eV. However in this case the shape of the observed spectrum [9, 10, 11, 12] is in disagreement with the theoretical predictions in Refs. [13, 14]. It is more difficult for sterile neutrinos to explain this spectral deformation, and so it seems likely that this anomaly is actually just a result of a faulty theoretical calculation of the reactor spectrum [15, 16]. Therefore, motivation for sterile neutrinos with a mass beneath 1 eV has evaporated, the region of interest for sterile neutrino masses is now that above 1 eV.

Such massive sterile neutrinos are in some tension with Planck CMB data [17]. However, assuming the standard Λ CDM cosmological model, the Planck data is in 3σ of tension with an every growing list of measurements, from Lyman α forest baryon acoustic oscillations [18] to the Hubble constant as determined by the local distance ladder [19]. While massive sterile neutrinos alone cannot eliminate these tensions [20, 21], they do ease the tension by increasing the uncertainties reported by Planck [17] and they may be part of a larger solution involving dynamic dark energy.

1.2 Sterile Neutrino Searches

Motivated by these anomalies, there have been a number of proposed experiments to search for sterile neutrinos. Most of these proposals search for sterile neutrinos in the disappearance channel $\bar{\nu}_e \rightarrow \bar{\nu}_e$. Experiments using research reactor neutrinos are at an advanced stage: some are already running [22], running with only one detector module [23] or about to start running [24].

Perhaps the most sensitive disappearance channel sterile neutrino searches use Isotope

Decay At Rest (IsoDAR). To our knowledge in all such proposals a neutron source produces neutrons which are absorbed by ${}^7\text{Li}$. This produces ${}^8\text{Li}$ whose decay produces $\bar{\nu}_e$ with a well known energy spectrum, extending to 13 MeV, with an average energy of 6.5 MeV. This canonical setup was first proposed in Ref. [25], in which the neutron source was a “special nuclear reactor”. After half a century, this idea has come full circle with proposals to use an accelerator driven system (ADS) subcritical reactor as the neutron source.

The most advanced proposals have been made by the DAE δ ALUS collaboration [26]. In these proposals a cyclotron accelerates a high intensity proton beam or a molecular beam which is then dissociated into a proton beam. The proton beam energy is 60 MeV with a current of 10 mA. The protons strike a beryllium target, creating spallation neutrons. In some cases the neutrons exit from the target into a heavy water moderator [27, 28], while in some cases there is no moderator [29]. In either case, they then enter into a sleeve containing isotopically pure ${}^7\text{Li}$, sometimes in the compound FLiBe (Li_2BeF_4) [29], where they are absorbed yielding ${}^8\text{Li}$. The eventual ${}^8\text{Li}$ decay creates $\bar{\nu}_e$ with a well-known energy spectrum.

IsoDAR disappearance channel experiments have several advantages over reactor neutrino experiments. First, the fact that the spectrum is fairly well known reduces a major source of error in reactor neutrino experiments. Second, 87% of the $\bar{\nu}_e$ have energies above 6 MeV. At these relatively high energies the accidental background that plagues reactor experiments is reduced by two orders of magnitude. Third, this higher energy means that the same distance to energy ratio L/E , and so the same oscillation phase, is achieved at greater distances. As a result more shielding can be added and, more crucially, distance resolution requirements are weakened. This also allows access to higher sterile neutrino masses.

To save money, all IsoDAR proposals use existing infrastructure, either the accelerator or the detector. In particular DAE δ ALUS has provided a detailed proposal for an IsoDAR experiment at KamLAND [29] and the JUNO collaboration has also included such an experiment in its plan [28]. In addition in Refs. [30, 31] IsoDAR experiments have been proposed using the LINACs that are being built for China’s Accelerator Driven System (ADS) subcritical reactor project. In particular, a 25 MeV, 10 mA proton accelerator will be complete this year, although for now perhaps only at 5 mA, and a 250-500 MeV, 10 mA accelerator called China Initial ADS (CI-ADS) will be completed in 2022, with civil engineering beginning this year. In the first case, a small detector would need to be built. CI-ADS on the other hand is near Daya Bay, and so may be able to transport and use Daya Bay detectors.

1.3 Summary of results

The target stations of all four of the above IsoDAR proposals are quite similar. In this paper we will present the results of our simulations of various modifications of these target stations. Our objective is to determine to what extent various modifications affect the $\bar{\nu}_e$ yield. In particular we will not be interested here in how these modifications may be implemented, on the effect on the sensitivity to sterile neutrino searches or other science goals or even on the absolute normalization of the $\bar{\nu}_e$ flux. As a result our study is quite straightforward, lending itself to simulation with FLUKA and also with GEANT4 using the physics list FTFP_BERT_HP below 250 MeV and QGSP_BIC_HP at 250 MeV.

These results will lead us to three main conclusions:

- 1) Mixing the moderator and the ^7Li converter [32] increases the $\bar{\nu}_e$ yield by as much as 50%.
- 2) In this mixed case, for a sufficiently large converter, the $\bar{\nu}_e$ rate can be estimated quite precisely using only the overall normalization of the neutron yield, the cross sections and a simple analytic formula.
- 3) In the case of the 250 MeV CI-ADS beam with the preferred W target, a gap between the target and the converter can reduce the neutrons lost by bounce-back into the target by as much as 30%.

We will organize our discussion by dividing the simulation into parts. First, in Sec. 2 we will describe the transport of neutrons in the converter and the resulting isotope production. This will be done in an idealized setting with no proton beam or target and a monochromatic neutron source. In Sec. 3 we will consider the proton beam striking the target and the creation of spallation neutrons. Finally in Sec. 4 we will describe our full simulations, from the proton beam to ^8Li production.

2 Neutron Transport

In this section we will consider the simpler problem of calculating the $\bar{\nu}_e$ rate given a monochromatic neutron source in the center of the converter which is surrounded by a graphite reflector. We will see that at the relevant energies, the $\bar{\nu}_e$ yield has little dependence on the neutron energy and, for a large enough converter, can easily be estimated analytically. We feel that the results in this section provide an intuitive understanding of the results of the full target station simulations which will be presented in Sec. 4.

2.1 Analytic Results

All of the converters which we will consider consist of H, D, Be, ^6Li , ^7Li , O and F, with O having the isotopic abundances found in nature. At the energies of interest the absorption cross sections are inversely proportional to the neutron velocity, and the elastic scattering cross sections are energy-independent up to about 1 MeV, where they begin to fall.

The vast majority of our neutrons will have initial energies between 100 keV and 5 MeV, and so we approximate the elastic scattering cross sections to be energy-independent. We will use the cross sections from Ref. [36] which are summarized in Table 1. All absorption cross sections are reported at 0.025 eV, to convert to other energies it suffices to scale inversely by the mean neutron velocity.

Let ρ_i be the number of isotopes of type i per unit volume and let $\sigma_{\text{elastic}}^i$ be the elastic scattering cross section for a neutron on an isotope of type i . Considering only elastic scattering, as is reasonable before the neutrons are thermalized, the mean free path is

$$\lambda = \frac{1}{\sum_i \rho_i \sigma^i}. \quad (2.1)$$

We will consider a simple model of neutron moderation in which the neutron loses 40% of its energy during each collision with a D, and no energy during the other collisions. In particular we will ignore elastic scattering with H which will be quite rare in the cases that follow as a result of the high isotopic purity of D. The probability that a given elastic scattering involves a D is equal to

$$p = \rho_D \sigma^D \lambda. \quad (2.2)$$

Therefore roughly every $1/p$ elastic scatterings there is an elastic scattering with a D. Let us assume that at each of these $1/p$ scatterings, as the target is much heavier than the neutron, the neutron's direction is randomized and so the neutron follows a 3-dimensional random walk. Therefore the neutron will travel, on average, a distance

$$d_D = \frac{\lambda}{\sqrt{3p}} = \sqrt{\frac{\lambda}{3\rho_D \sigma^D}} \quad (2.3)$$

in each direction between two elastic scatterings with D.

A neutron which is created with an energy of E MeV will thermalize to room temperature after $-\ln(4E \times 10^7)/\ln(0.6)$ collisions with D. During these collisions, it will travel an expected distance of

$$d_{\text{therm}} = \sqrt{\frac{\lambda \ln(4E \times 10^7)}{3 \ln(5/3) \rho_D \sigma^D}} \quad (2.4)$$

	H	D	⁶ Li	⁷ Li	Be	O	F
σ_{elastic} (barns)	82.03	7.64	0.97	1.4	7.63	4.232	4.018
σ_{abs} (barns)	0.3326	5.19×10^{-4}	940	0.0454	0.0076	1.9×10^{-4}	0.0096

Table 1: Elastic scattering and absorption cross sections of various isotopes.

	Li	LiOD	LiOD·D ₂ O	solution	FLiBe
density (gm/cm ³)	0.534	1.52 [33]	1.62 [33]	1.1	1.94 [34]
ρ_{H} (cm ⁻³)	0	3.66×10^{20}	6.50×10^{20}	6.16×10^{20}	0
ρ_{D} (cm ⁻³)	0	3.62×10^{22}	6.44×10^{22}	6.10×10^{22}	0
ρ_{Li} (cm ⁻³)	4.59×10^{18}	3.66×10^{18}	2.17×10^{18}	3.24×10^{17}	2.36×10^{18}
ρ_{Li} (cm ⁻³)	4.59×10^{22}	3.66×10^{22}	2.17×10^{22}	3.24×10^{21}	2.36×10^{22}
ρ_{Be} (cm ⁻³)	0	0	0	0	1.18×10^{22}
ρ_{O} (cm ⁻³)	0	3.66×10^{22}	4.34×10^{22}	3.58×10^{22}	0
ρ_{F} (cm ⁻³)	0	0	0	0	4.72×10^{22}

Table 2: Densities and isotope number densities in various converters. The densities have been rescaled from the original references to reflect the desired isotope compositions.

in each direction.

We now make the reasonable approximation that neutrons can only be absorbed after they have thermalized. The probability that an interaction after thermalization leads to absorption is

$$p_{\text{abs}} = \frac{\sum_i \rho_i \sigma_{\text{abs}}^i}{\sum_i \rho_i (\sigma_{\text{elastic}}^i + \sigma_{\text{abs}}^i)}. \quad (2.5)$$

Therefore one expects that after thermalization a neutron will scatter $1/p_{\text{abs}}$ times before being absorbed, during which it travels an expected distance of

$$d_{\text{abs}} = \frac{\lambda}{\sqrt{3p_{\text{abs}}}} \quad (2.6)$$

in each direction. We will make the rough approximation that λ is the same before and after thermalization.

Thermalized neutrons in general will be absorbed in the converter. The probability that a thermalized neutron is absorbed by ⁷Li and therefore yields a $\bar{\nu}_e$ is

$$p_{\nu} = \frac{(\rho_{\text{Li}}) (\sigma_{\text{abs}}^{\text{Li}})}{\sum_i \rho_i \sigma_{\text{abs}}^i}. \quad (2.7)$$

We will be interested in five different converter materials. In each the D will be 99% isotopically pure, with the remaining 1% being H. Also the ⁷Li will be 99.99% isotopically

	Li	LiOD	LiOD·D ₂ O	solution	FLiBe
λ (cm)	15.5	1.95	1.32	1.52	3.20
p	0	0.540	0.648	0.709	0
d_D (cm)	∞	1.53	0.945	1.04	∞
d_{therm} (cm) $E = 1$	∞	8.96	5.53	6.10	∞
d_{abs} (cm)	29.8	11.2	11.6	27.5	16.8
p_ν	0.326	0.317	0.300	0.208	0.280

Table 3: Neutron transport properties of each converter

pure, with the remaining 0.01% consisting of ^6Li . In practice the vendors with whom we have spoken offer much lower prices if there are some other impurities, however these other impurities are irrelevant here due to their low neutron absorption cross sections. The five materials are pure metallic Li, LiOD, LiOD·D₂O, a heavy water solution which is 11.6% LiOD by mass and finally FLiBe. The first material has been chosen in most IsoDAR proposals [27], the last in IsoDAR at KamLAND [29], and the others have been suggested in Ref. [32].

Each compound can have various densities and bulk densities depending on the crystalline structure and/or preparation. We have chosen not to optimize these densities, but rather we have chosen the densities which appear most often on the web pages of vendors, as these are likely to be the most readily available. These densities were then rescaled to the isotope specifications of interest for our study. The results are summarized in Table 2. In the case of the heavy water solution we simply used the density of heavy water. The density of metallic lithium has an appreciable temperature dependence, and we have used a density corresponding to room temperature.

Combining the number densities ρ_i in Table 2, together with the cross sections in Table 1, one can now evaluate the various quantities above for each converter. The results are shown in Table 3. As we have made the approximation that only D moderates, the thermalization distance for the metallic Li and the FLiBe converters can not be evaluated. In the other cases, the longest distance is the absorption distance d_{abs} which is approximately 11 cm for LiOD and LiOD·D₂O and 27 cm for the solution. As a result, one expects that the ^8Li production, and so the $\bar{\nu}_e$ production per neutron will saturate to p_ν when the converter radius is much greater than 11 cm or 27 cm respectively. The saturation value p_ν is much less for the solution, but comparable for the other converters.

The fact that p_ν is close to 1/3 is easy to understand. There is 10^4 times more ^7Li as ^6Li in each case, but σ_{abs} of ^6Li is 2×10^4 times higher than that of ^7Li . Therefore ^6Li absorbs

twice as many neutrons as ${}^7\text{Li}$, leaving about 1/3 of the neutrons for ${}^7\text{Li}$. If on the other hand the ${}^7\text{Li}$ purity is increased to 99.995% as in Ref. [29], then the same argument implies that p_ν will be about 1/2, corresponding to a 50% increase in the $\bar{\nu}_e$ yield. We hope that the optimizations described in this note may lead to a smaller, more efficient converter which in turn would allow, at the same price, a higher isotopic purity of Li and so a higher $\bar{\nu}_e$ yield.

2.2 Simulation Results

We have simulated neutron transport using all of these converters with FLUKA [38] and some of these also with GEANT4 [37]. Each FLUKA configuration was simulated with at least 10^5 monochromatic neutrons per energy, meaning that statistical fluctuations are negligible. Our configurations consist of concentric cylinders. In the center is a vacuum with a 10 cm radius and a length of 20 cm. In the case of metallic lithium, following the DAE δ ALUS proposal [27], this is surrounded by 5 cm of heavy water on each side. Next is the converter, which extends $10n$ cm beyond the vacuum where we have run simulations for integral values of n . In the case of the solution instead we consider 40, 80, 100, 120, 140, 160 and 180 cm of extension beyond the vacuum. In every case this is surrounded by 60 cm of graphite on each side. For simplicity we have not included cooling systems.

The results of our simulations, for neutrons at energies of 0.25 MeV, 0.8 MeV, 2.5 MeV, 8 MeV, 25 MeV and 80 MeV, are shown in Fig. 1 for various quantities of ${}^7\text{Li}$. The cost of the converter is driven by the pure ${}^7\text{Li}$ and so it is reasonable to compare converters at fixed ${}^7\text{Li}$ mass.

One may observe that on the right side of each panel, as the Li mass is sufficient to thermalize and absorb the neutrons, in general the ${}^8\text{Li}$ production, which is equal to the $\bar{\nu}_e$ production, reaches an asymptotic value. This asymptotic value agrees well with p_ν calculated in Eq. (2.7) in every case except for the GEANT4 simulation of the solution, which tends to be about 4% too high. Note that at energies above 2.5 MeV there is no asymptotic value, instead the ${}^8\text{Li}$ production continues to increase as the converter size is increased. This is because at these energies the neutrons have sufficient energy to break the D or Be in the converter, freeing more neutrons. The neutron increase at these high energies is therefore a result of neutron multiplication. While this neutron multiplication is significant at energies of 25 MeV and above, we will see that even 250 MeV protons create very few neutrons above 5 MeV, and so neutron multiplication in fact is insignificant in every case that we will consider. It is most significant for FLiBe, as a result of the lower energy cost to remove a valence neutron from ${}^9\text{Be}$ with respect to, for example, D. In fact, we have run additional simulations with fictional converter materials that have a higher Be density

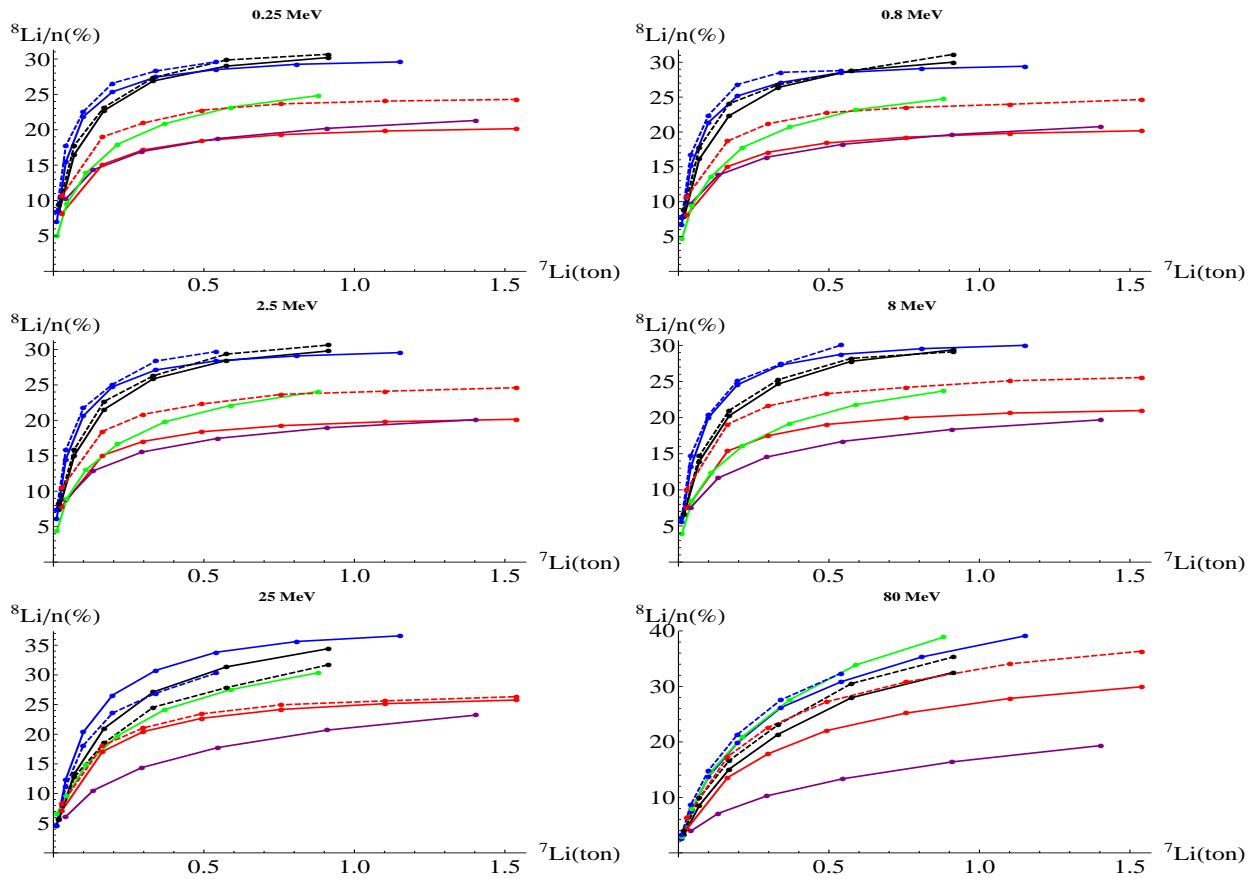


Figure 1: The $^8\text{Li}/\text{neutron}$ ratio for monochromatic neutrons at various energies. The black, blue, red, purple and green curves represent the LiOD, LiOD·D₂O, solution, metallic Li and FLiBe converters respectively. Solid curves were produced with FLUKA and dashed curves with GEANT4. The horizontal axis is the mass of the ^7Li .

and we have found that at 60 MeV they outperform all of the materials considered here.

The main result of our paper is quite clear in every panel of Fig. 1. The metallic Li converter outside of a heavy water moderator, which has been chosen at many IsoDAR experiments [27], in fact has an appreciably lower neutron yield than the two other solid converters considered. This is true for every neutron energy, and so it will be true for every proton beam. The effect is quite large, it suggests that by mixing the moderator and the converter one may increase the $\bar{\nu}_e$ flux by as much as 50%. This result has been anticipated in Ref. [32], although quantitatively our simulation results are quite different from theirs [35].

3 Neutron Production

IsoDAR experiments begin with a proton beam, which strikes a target creating neutrons which are then absorbed by various isotopes. Those absorbed by ${}^7\text{Li}$ provide ${}^8\text{Li}$ and so our $\bar{\nu}_e$ signal. In Sec. 2 we studied the second step of this experiment, the neutron transport and absorption. In this section we will instead describe the first step, the production of neutrons at the target.

In each case, throughout this paper, the target will be 20 cm long with a 10 cm radius. We have optimized the target dimensions in each case and found that this standard size yields a ${}^8\text{Li}$ production rate which is always near the optimum, and so for simplicity we report only simulations with this fixed size. The 25 MeV and 60 MeV proton beams always strike a Be target, whereas we consider heavy metal targets for the 250 MeV beam, as these produce a higher neutron yield above about 50 MeV.

We have simulated this production with GEANT4 and FLUKA and we have compared our results with experimental data at various energies up to 100 MeV [39, 40] and also with the simulations of Ref. [41] at 250 MeV. In general we have found that the GEANT4 simulations yield 10-20% less neutrons than experimental data and the FLUKA simulations 20-40% less, whereas we found better than 1% agreement with the simulations of Ref. [41]. The deficit in neutron production in FLUKA arises entirely at low energies.

Including the latest data it is possible to improve the GEANT4 simulations considerably [29]. However one of the main results of Sec. 2 is that below about 25 MeV the initial neutron energy has little effect on the isotope production. In Fig. 2 we plot the normalized cumulative distributions of the neutron spectra produced by 25 MeV, 60 MeV and 250 MeV proton beams, as determined by FLUKA.

As can be seen in Fig. 2, in each case less than 10% of the neutrons have energies in excess of 25 MeV. Therefore the shape of the neutron spectrum will have very little effect

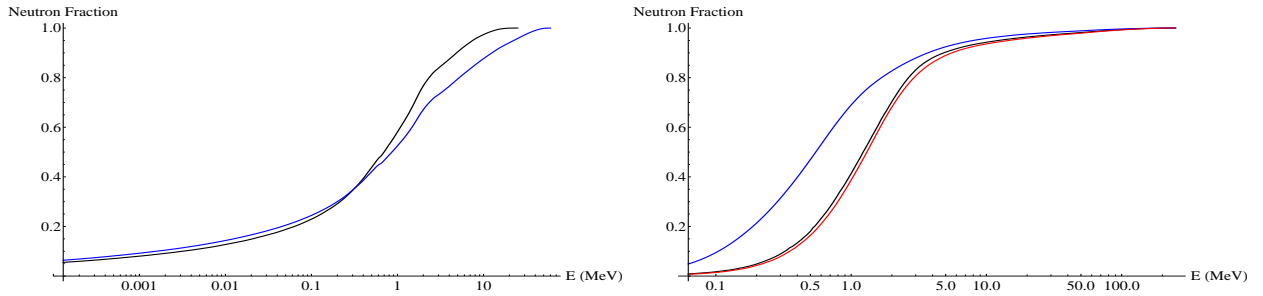


Figure 2: The normalized cumulative distribution of the neutron energies as produced using a 25 MeV (left panel, black), 60 MeV (left panel, blue) and 250 MeV (right panel) proton beam. The y -axis is the fraction of neutrons beneath a specific energy. On the left panel a Be target is used, while on the right panel Pb (black), W (blue) and Bi (red) targets are used.

on the final ${}^8\text{Li}$ yield. This means that for our study of the effect of target station design on the ${}^8\text{Li}$ yield, we only need the total normalizations of the neutron flux and not the detailed spectral shape below 10 MeV. This justifies our use of unmodified GEANT4 and FLUKA in this note: FLUKA and GEANT4 underestimate the neutron flux significantly but the missing neutrons are at energies well below the neutron multiplication threshold, where the neutron energy and so the spectral shape does not affect the ${}^8\text{Li}$ yield.

4 The Full Simulation

In this subsection we simulate the full experimental setup, from the proton beam to the ${}^8\text{Li}$ production. Note that the result cannot simply be obtained by folding the results of Sec. 3 into Sec. 2 because neutrons can bounce from the converter back into the target, where they may be absorbed. This bounce-back process is only possible in a simulation which includes both the target and the converter. In particular, we will see that bounce-back is most important for W targets, which have the highest probability of absorbing the neutrons. On the other hand it is nearly negligible for the other targets. The W target nonetheless is important as a granular W target is currently the favored target for the CI-ADS 250 MeV beam, even if the beam energy is increased to 500 MeV.

As FLUKA predicts lower spallation neutron yields than have been observed in experiment, one may expect that the true ${}^8\text{Li}$ yields will be 20-40% greater than those reported below in each case.

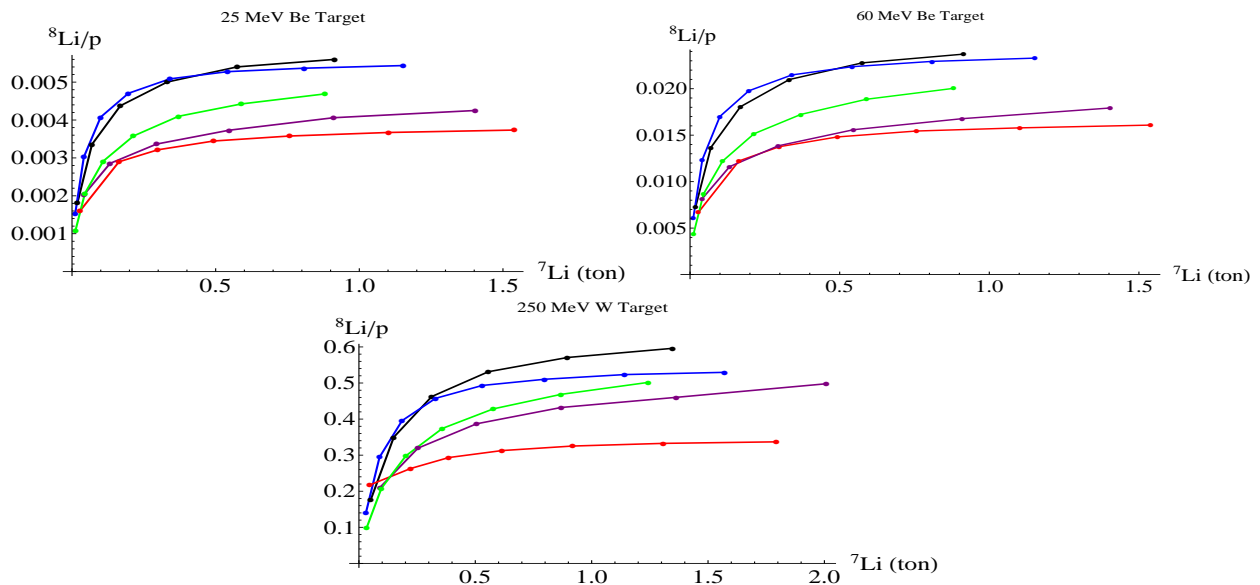


Figure 3: The ^8Li production given a 25 MeV, 60 MeV and 250 MeV proton beam is shown in the three panels as a function of the ^7Li mass. The target is always a cylinder of length 20 cm and radius 10 cm. At 25 MeV and 60 MeV the target is Be. At 250 MeV the target is W and it is surrounded by a 10 cm vacuum sleeve. The converters are LiOD (black), LiOD·D₂O (blue), the solution (red), metallic Li (purple) and FLiBe (green). In the case of metallic Li, a 5 cm heavy water moderator is placed inside the converter.

4.1 Comparison of converters

In this subsection we compare various converter designs. As bounce-back results in significant neutron loss in the case of a W converter, the target has been surrounded with a 10 cm gap in this case. To increase the yield of the metallic Li converter, 5 cm of heavy water moderator has been placed between the target and the converter in this case, following the design in Ref. [27].

The results are shown in Fig. 3. Our main result is apparent here, the converters in which Li is mixed with a deuterium moderator significantly outperform the others.

4.2 Liquid nitrogen cooling

As can be seen in Table 3, the longest distance that neutrons need to travel is d_{abs} , the distance traveled between thermalization and absorption. The ^8Li to proton ratio approaches p_ν when the size of the converter is several times d_{abs} . Therefore d_{abs} sets the scale of the

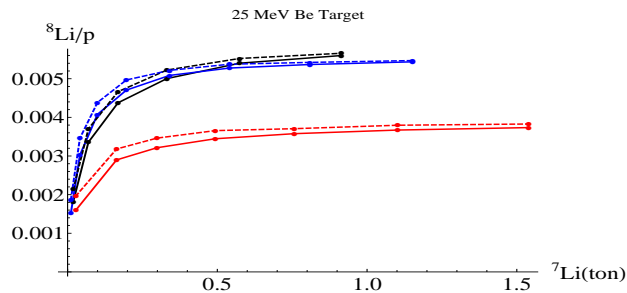


Figure 4: The ^8Li yield per 25 MeV proton as a function of the ^7Li mass. The black, blue and red curves correspond to LiOD, LiOD·D₂O and the solution respectively. The solid (dashed) curves correspond to a room temperature (liquid nitrogen cooled) converter.

converter and is responsible for the reduction in ^8Li generation when the converter is smaller than that scale. As a result, a smaller d_{abs} would allow for a smaller converter with the same p_ν or a larger p_ν with the same size converter.

The length scale d_{abs} is, according to Eqs. (2.5) and (2.6), inversely proportional to the square root of the absorption cross sections σ_{abs}^i . These in turn are inversely proportional to the neutron velocity, and so to the square root of the neutron temperature. This means that if the converter temperature is reduced by a factor of 4, by cooling with liquid nitrogen, then the neutron velocities will be reduced by a factor of 2 and so d_{abs} will be reduced by a factor of $\sqrt{2}$, allowing for an increased ^8Li yield with a smaller and cheaper target station.

We have rerun our simulations with the converter at liquid nitrogen temperature, again without including any cooling system in our design. In practice the 60 MeV and 250 MeV experiments are likely to have enough money to buy large converters, and so for brevity we only report our results in the case of the 25 MeV proton beam in Fig. 4, although the cooling has a similar effect at other temperatures. As expected based on the general arguments above, liquid nitrogen cooling has only a modest effect on the ^8Li production. However, in general it leads to a ^8Li production with a mass M of ^7Li equal to that which would be obtained with a mass of about $2M$ of room temperature ^7Li . This corresponds to an improvement which is quite small for large ^7Li converter masses, but approaches 20% when the ^7Li mass is less than 100 kg.

4.3 Vacuum sleeve

In every setup, a considerable fraction of the neutrons bounce back into the target. However only the W target has a sufficiently high neutron absorption cross section to absorb an

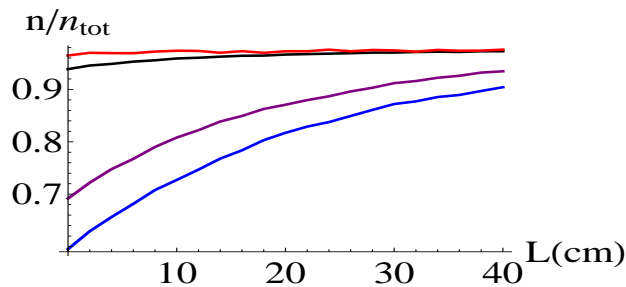


Figure 5: The fraction of neutrons that are not lost to neutron bounce-back, in the case of a 250 MeV proton beam, as a function of the size of the gap between the target and the converter. The red, black, purple and blue curves correspond to a Bi target with a LiOD·D₂O converter, a Pb target with a LiOD·D₂O converter, a W target with a LiOD converter and a W target with a LiOD·D₂O converter.

appreciable fraction of these neutrons. Nonetheless, a W target is currently favored for the CI-ADS 250 MeV accelerator, and so this case cannot be ignored.

If there is a gap between the target and the converter, then some of the neutrons bouncing back from the converter will fly through the gap and reenter the converter elsewhere without ever entering the target. As a result, a gap reduces the number of neutrons lost to bounce-back. In Fig. 5 we plot the results of FLUKA simulations of the fraction of neutrons which leave the target and are not reabsorbed in the target later, as a function of the gap size.

One can observe that in the case of the LiOD·D₂O converter, more neutrons are lost to bounce-back than in the case of the LiOD converter. We have verified that this is a consequence of more neutrons bouncing back, and not of the energy spectrum of the bounced-back neutrons.

The main result of this study is that bounce-back can lead to a loss of as many as 40% of the neutrons. However, with a sufficiently large gap, this loss can be made as small as desired. Of course, a large gap also implies that a greater quantity of ⁷Li is needed for the same converter thickness. It also means that the $\bar{\nu}_e$ are created over a larger physical area, leading to a greater baseline uncertainty which reduces the sensitivity of a sterile neutrino experiment at large ΔM^2 .

5 Conclusions

In our opinion, IsoDAR experiments provide the most powerful feasible tests of sterile neutrino models that have been invoked to explain observed anomalies. Several such experiments have been proposed at laboratories around the world.

In this note we have simulated three proposed methods for increasing the $\bar{\nu}_e$ yield of these experiments. In the first, the ${}^7\text{Li}$ converter is mixed with a D moderator. In the second, the converter is cooled to liquid nitrogen temperatures. In the third, a gap is placed between the target and the converter. We have not investigated the feasibility of these modifications. In particular, our simulations were quite idealized as we did not include a support structure for a target separated by a gap, nor cooling for the target or for the converter. We also did not include the impurities such as K which are normally included in isotopically pure ${}^7\text{Li}$ available on the market.

We have found that the utility of each of these modifications depends on the experimental setup. For example, the purpose of the gap is to allow bounced-back neutrons to reenter the converter without passing through the target where they may be absorbed. However, only the W target has a sufficiently high absorption cross section for bounced-back neutrons to significantly affect the $\bar{\nu}_e$ yield. Therefore we have found that the gap is only useful in the case of the W target. However it is quite likely that the 250 MeV CI-ADS beam will use a W target, therefore it seems likely that one will wish to incorporate this gap in the target station design for any IsoDAR experiment at that beam.

The liquid nitrogen cooling reduces the fraction of neutrons that escape the converter and the reflector to the outside. The fraction of escapes which are prevented is significant. However such neutron escapes are themselves only significant in the case of a thin moderator, in particular if less than 100 kg of Li is used. Such a thin moderator would only be used either to save money, or so as to be able to obtain a higher purity at the same price. For a very thin moderator, the increase in $\bar{\nu}_e$ yield at liquid nitrogen temperatures approaches 20%. However, given the hot target in the center of the target station, appreciable cooling of the converter may be impractical. In fact, it may be that the converter is appreciably above room temperature, in which case more neutrons will escape than we have simulated and so the converter will need to be larger. We need to insure however that the converter does not become too hot, as some of these converters will thermally decompose [42]. In the future we intend to perform more detailed simulations, including heat dissipation, to resolve this issue.

Perhaps our main result is that we have confirmed the claims of Ref. [32] that mixing the

converter with a D moderator improves the neutron capture rate appreciably. As a result, for Li masses of order a ton or less, neutrons can thermalize anywhere in the converter volume and so far less neutrons escape, increasing the $\bar{\nu}_e$ yield considerably with respect to the metallic Li converter outside of a thin moderator proposed in Ref. [27].

In this article we have determined how several modifications of the core IsoDAR target station design can potentially affect the $\bar{\nu}_e$ yield. In the future, to drive these proposals further, we will investigate both their practicality and also their effects on the physics goals of IsoDAR experiments. To do this, we will require simulations which correctly reproduce the shape of the neutron energy spectrum and its angular distribution and also model the target station heating and cooling.

Acknowledgement

We thank M. Osipenko for discussions and advice. JE and EC are supported by NSFC grant 11375201. EC is also supported by the Chinese Academy of Sciences President's International Fellowship Initiative grant 2015PM063. MD is supported by the Chinese Academy of Sciences President's International Fellowship Initiative grant 2016PM043.

References

- [1] C. Athanassopoulos *et al.* [LSND Collaboration], “Measurements of the reactions C-12 (electron-neutrino, e-) N-12 (g.s.) and C-12 (electron-neutrino, e-) N*-12,” Phys. Rev. C **55** (1997) 2078 [nucl-ex/9705001].
- [2] A. Aguilar-Arevalo *et al.* [LSND Collaboration], “Evidence for neutrino oscillations from the observation of anti-neutrino(electron) appearance in a anti-neutrino(muon) beam,” Phys. Rev. D **64** (2001) 112007 [hep-ex/0104049].
- [3] B. Armbruster *et al.* [KARMEN Collaboration], “Upper limits for neutrino oscillations muon-anti-neutrino \rightarrow electron-anti-neutrino from muon decay at rest,” Phys. Rev. D **65** (2002) 112001 [hep-ex/0203021].
- [4] M. Antonello *et al.* [ICARUS Collaboration], “Search for anomalies in the ν_e appearance from a ν_μ beam,” Eur. Phys. J. C **73** (2013) 2599 [arXiv:1307.4699 [hep-ex]].
- [5] A. A. Aguilar-Arevalo *et al.* [MiniBooNE Collaboration], “Improved Search for $\bar{\nu}_\mu \rightarrow \bar{\nu}_e$ Oscillations in the MiniBooNE Experiment,” Phys. Rev. Lett. **110** (2013) 161801 [arXiv:1207.4809 [hep-ex], arXiv:1303.2588 [hep-ex]].

- [6] W. Hampel *et al.* [GALLEX Collaboration], “Final results of the Cr-51 neutrino source experiments in GALLEX,” *Phys. Lett. B* **420** (1998) 114.
- [7] J. N. Abdurashitov *et al.* [SAGE Collaboration], “Measurement of the solar neutrino capture rate with gallium metal. III: Results for the 2002–2007 data-taking period,” *Phys. Rev. C* **80** (2009) 015807 [arXiv:0901.2200 [nucl-ex]].
- [8] G. Mention, M. Fechner, T. Lasserre, T. A. Mueller, D. Lhuillier, M. Cribier and A. Letourneau, “The Reactor Antineutrino Anomaly,” *Phys. Rev. D* **83** (2011) 073006 [arXiv:1101.2755 [hep-ex]].
- [9] S. B. Kim, “Observation of Reactor Antineutrino Disappearance at RENO,” talk given on June 4, 2012 at *Neutrino 2012* in Kyoto
- [10] S. H. Seo [RENO Collaboration], “New Results from RENO and The 5 MeV Excess,” *AIP Conf. Proc.* **1666** (2015) 080002 [arXiv:1410.7987 [hep-ex]].
- [11] Y. Abe *et al.* [Double Chooz Collaboration], “Improved measurements of the neutrino mixing angle θ_{13} with the Double Chooz detector,” *JHEP* **1410** (2014) 086 [*JHEP* **1502** (2015) 074] [arXiv:1406.7763 [hep-ex]].
- [12] D. V. Naumov [Daya Bay Collaboration], “Recent results from Daya Bay experiment,” *EPJ Web Conf.* **95** (2015) 04043 [arXiv:1412.7806 [hep-ex]].
- [13] T. A. Mueller *et al.*, “Improved Predictions of Reactor Antineutrino Spectra,” *Phys. Rev. C* **83** (2011) 054615 [arXiv:1101.2663 [hep-ex]].
- [14] P. Huber, “On the determination of anti-neutrino spectra from nuclear reactors,” *Phys. Rev. C* **84** (2011) 024617 Erratum: [*Phys. Rev. C* **85** (2012) 029901] [arXiv:1106.0687 [hep-ph]].
- [15] A. A. Zakari-Issoufou *et al.* [IGISOL Collaboration], “Total Absorption Spectroscopy Study of ^{92}Rb Decay: A Major Contributor to Reactor Antineutrino Spectrum Shape,” *Phys. Rev. Lett.* **115** (2015) 10, 102503 [arXiv:1504.05812 [nucl-ex]].
- [16] D. A. Dwyer and T. J. Langford, “Spectral Structure of Electron Antineutrinos from Nuclear Reactors,” *Phys. Rev. Lett.* **114** (2015) 1, 012502 [arXiv:1407.1281 [nucl-ex]].
- [17] P. A. R. Ade *et al.* [Planck Collaboration], “Planck 2015 results. XIII. Cosmological parameters,” arXiv:1502.01589 [astro-ph.CO].

- [18] T. Delubac *et al.* [BOSS Collaboration], “Baryon acoustic oscillations in the Ly forest of BOSS DR11 quasars,” *Astron. Astrophys.* **574** (2015) A59 [arXiv:1404.1801 [astro-ph.CO]].
- [19] A. G. Riess *et al.*, “A 2.4% Determination of the Local Value of the Hubble Constant,” arXiv:1604.01424 [astro-ph.CO].
- [20] J. Evslin, “Model-Independent Dark Energy Equation of State from Unanchored Baryon Acoustic Oscillations,” To appear in *Phys. Dark Univ.* arXiv:1510.05630 [astro-ph.CO].
- [21] J. Evslin, “Isolating the Lyman Alpha Forest BAO Anomaly,” arXiv:1604.02809 [astro-ph.CO].
- [22] G. Boireau *et al.* [NUCIFER Collaboration], “Online Monitoring of the Osiris Reactor with the Nucifer Neutrino Detector,” *Phys. Rev. D* **93** (2016) no.11, 112006 doi:10.1103/PhysRevD.93.112006 [arXiv:1509.05610 [physics.ins-det]].
- [23] I. Michiels, “SoLid: Search for Oscillation with a 6Li Detector at the BR2 research reactor,” arXiv:1605.00215 [physics.ins-det].
- [24] V. Helaine, “Sterile neutrino search at the ILL nuclear reactor: the STEREO experiment,” arXiv:1604.08877 [physics.ins-det].
- [25] L. A. Mikaelian, P. E. Spivak and V. G. Tsinoev, “The proposal of experiments on low energy antineutrino physics,” *Nucl. Phys.* **70** (1965) 574.
- [26] J. Alonso, F. T. Avignone, W. A. Barletta, R. Barlow, H. T. Baumgartner, A. Bernstein, E. Blucher and L. Bugel *et al.*, “Expression of Interest for a Novel Search for CP Violation in the Neutrino Sector: DAE δ ALUS,” arXiv:1006.0260 [physics.ins-det].
- [27] A. Bungau *et al.*, “Proposal for an Electron Antineutrino Disappearance Search Using High-Rate ^8Li Production and Decay,” *Phys. Rev. Lett.* **109** (2012) 141802 [arXiv:1205.4419 [hep-ex]].
- [28] F. An *et al.* [JUNO Collaboration], “Neutrino Physics with JUNO,” *J. Phys. G* **43** (2016) no.3, 030401 [arXiv:1507.05613 [physics.ins-det]].
- [29] M. Abs *et al.*, “IsoDAR@KamLAND: A Conceptual Design Report for the Technical Facility,” arXiv:1511.05130 [physics.acc-ph].
- [30] E. Ciuffoli, J. Evslin and F. Zhao, “Neutrino Physics with Accelerator Driven Subcritical Reactors,” *JHEP* **1601** (2016) 004 [arXiv:1509.03494 [hep-ph]].

- [31] W. L. Zhan, “Accelerator Driven Sustainable Fission Energy,” Talk given at IPAC 2016, Busan, South Korea, May 8-13, 2016.
- [32] V. I. Lyashuk and Y. S. Lutostansky, “Reactor neutrons-antineutrino converter on the basis of lithium compounds and their solutions,” *Soviet Atomic Energy* **69** (1990) 696.
- [33] These densities were taken from the density of the Centers for Disease Control and Prevention: <http://www.cdc.gov>
- [34] D. T. Ingersoll, E. J. Parma, C. W. Forsberg, and J. P. Renier, “Core Physics Characteristics and Issues for the Advanced High Temperature Reactor (AHTR),” Proceedings of ARWIF 2005, Oak Ridge National Laboratory, Feb 16-18, 2005.
- [35] V. I. Lyashuk and Y. S. Lutostansky, “Intensive neutrino source on the base of lithium converter,” arXiv:1503.01280 [physics.ins-det].
- [36] V. F. Sears, “Neutron scattering lengths and cross sections,” *Neutron News* **3** (1992) 26.
- [37] S. Agostinelli *et al.* [GEANT4 Collaboration], “GEANT4: A Simulation toolkit,” *Nucl. Instrum. Meth. A* **506** (2003) 250.
- [38] G. Battistoni, S. Muraro, P. R. Sala, F. Cerutti, A. Ferrari, S. Roesler, A. Fassò, J. Ranft, Proceedings of the Hadronic Shower Simulation Workshop 2006, Fermilab 6-8 September 2006, M. Albrow, R. Raja eds., AIP Conf Proceedings **896** (2007) 31. “FLUKA: a multi-particle transport code” A. Ferrari, P. R. Sala, A. Fassò, and J. Ranft, CERN-2005-10 (2005), INFN/TC_05/11, SLAC-R-773
- [39] I. Tilquin *et al.*, “Experimental Measurements of Neutron Fluxes Produced by Proton Beams (23-80 MeV) on Be and Pb Targets,” *Nucl. Instrum. Meth. A* **545** (2005) 339.
- [40] M. Osipenko *et al.*, “Measurement of neutron yield by 62 MeV proton beam on a thick Beryllium target,” *Nucl. Instrum. Meth. A* **723** (2013) 8 [arXiv:1302.7226 [nucl-ex]].
- [41] X. Zhang *et al.*, “Neutron production for 250 MeV protons bombarding on thick grain-made tungsten target,” *Eur. Phys. J. A* **51** (2015) no.8, 106.
- [42] H. Kudo, “The rates of thermal decomposition of LiOH(s), LiOD(s) and LiOT(s),” *J. Nucl. Mat.* **87** (1979) 185.